NASA Contract Final Report
NASW-4610
Planetary Geomorphology

Michael C. Malin
Principal Investigator

Malin Space Science Systems
P. O. Box 910148
San Diego, CA 92191-0148

SUMMARY OF RESEARCH

Mars Environmental Simulation Chamber

The Mars Environmental Simulation Chamber (MESC) at Malin Space Science Systems (MSSS) consisted of a 1 m diameter, 1.3 m tall experiment chamber capable of supporting a 2 mb CO_2 atmosphere, housed inside a 2.7 x 3.5 x 2.6 m walk-in freezer capable of maintaining a temperature of -30° C. The chamber effectively simulated the surface conditions of Mars at low- to mid-latitudes. An IBM-compatible computer with a 10-bit DAC card ran the experiment.

Prior to loss of funding in July 1993, the chamber was being refurbished and its data system expanded for the set of experiments that had been proposed and funded in FY 92. Altadena Instruments Corporation, working under subcontract, took the lead in developing the system architecture, redesigning the data acquisition system as needed, and implementing the system.

One of the major problems in the series of ice runs was that the subsurface temperature probes did not function. AIC re-evaluated the design and, after testing several suitable sensors, installed 50 type T thermocouples, each 2 m long. In this design, each thermocouple was soldered to a rectangular copper foil spreader 0.3 cm wide by 2.8 cm long to ensure an accurate reading. The long rectangular shape was used because it had a large area for good thermal connection to the test material. In this design, sample materials could be contained either in the full diameter chamber, or in a large cardboard cylinder that could be placed inside the chamber as a means of conserving materials. Holes drilled in the cardboard cylinder allowed a "straw" to reach to both sides. The thermocouple assembly then was slid into the straw to the desired point. The cylinder was then filled with sample material until it grazed the bottom of the straw. The straw was then removed, from the far side (the side away from the leads), leaving the thermocouple in place. More material could then be added, repeating the addition of thermocouples as required, until the sample was the requisite thickness. After each test condition, additional thermocouples and material could be added and the next test conducted. Tools for deploying the thermocouples were designed, built, and their function verified by test.

An infrared radiometer (8-14 μm band) was also installed in the chamber. The mounting scheme permited the radiometer to view not only the surface of the test sample, but to be deployed by remote, computer command to view a calibration target within the chamber. The radiometer was covered with a spaceflight-like thermal blanket and used two small heaters from the Mars Observer Camera thermal/vacuum test equipment for thermal control. Operation and calibration were confirmed.

Software was written to digitize the analog output of the thermocouples and to take these digital signals and those produced by the radiometer, provide appropriate conditioning and calibration, and create a file format that could be accepted by existing analysis tools.

Additional facility modifications were necessary to provide power to the chamber. At the time funding was cut off, work had begun on integrating the radiometer control, thermistor readout, and lamp control into a single computer-controlled system. Approximately four weeks of vacuum and low pressure $C0_2$ tests remained to be completed in order to isolate the residual vacuum leaks and to debug the control electronics and software under actual operating conditions.

Following two unsuccessful attempts to regain support for this work, the MESC was disassembled and given to the Jet Propulsion Laboratory, where it is being used to test hardware designs for future Mars exploration equipment.

Science Results

The following paragraphs describe some of the science results derived from the MESC.

The apparatus in which experiments on 1 m by 50 cm thick samples of H_2O ice and ice covered with non-volatile particles were conducted in a Mars-like environment (3 mb of CO2 at ~250 °K) differed in only very slight ways from that described above (see, e.g., Moore and Malin, 1988, Moore, 1989, and Moore, 1990).

The experiments investigated the properties of pure 0.25-5.0 mm granular ice with a bulk density of about 0.5 gm/cm^3, covered with increasingly thick layers of 10 μm-sized dust or 200 μm-sized sand.

One clean-ice, four dust-covered (1, 2.5, 5, and 10 mm thick), and four sand experiments were conducted. During each experiment the sublimation rate was determined for four environmental conditions, described in Table 1. The sample was allowed to return to an isothermal state between the third and fourth conditions. The results of these experiments are shown in Figure 1 (see also Moore, 1990).

Table 1: Environmental Test Conditions

	Experiment Condition	Environment Equivalent
1	isothermal sample with the circulation pump off	None (baseline)
2	isothermal sample with the circulation pump on	Wind advection only
3	sample heated from above for one 24-hour period with the circulation pump off	Solar insolation only (no wind)
4	sample heated from above with the circulation pump on.	Solar insolation and wind advection

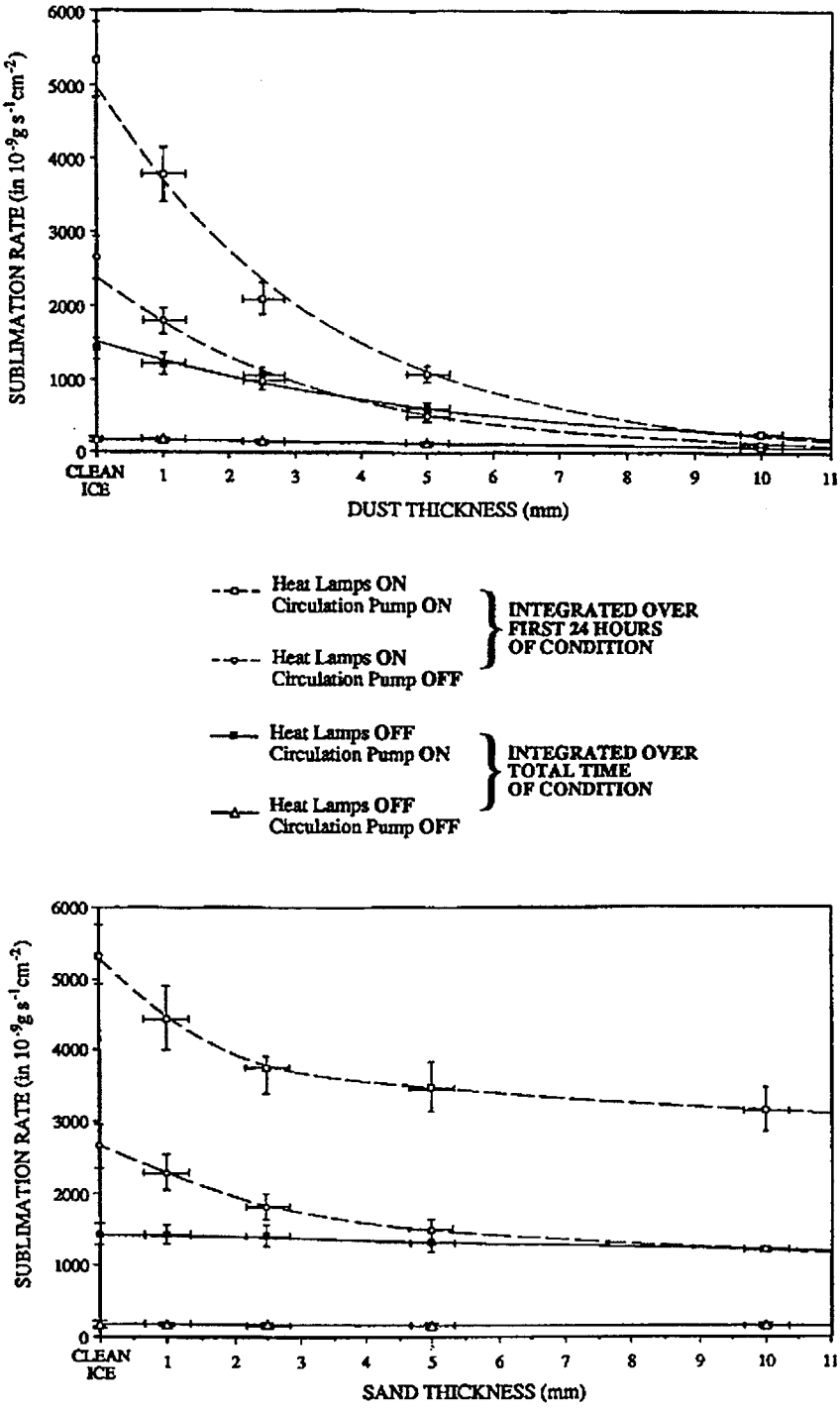

Figure 1: Sublimation rate as function of surficial mantle particle size (top and bottom graphs) and mantle thickness for four experimental conditions (top curves are Condition 4, bottom curves are Condition 1 in Table 1)

Condition 4 in each graph indicates that uncontrolled environmental factors had a negligible effect on the parameters under study. Condition 3 (wind advection only) shows a modest particle-size dependence, with smaller mantle particles inhibiting ice sublimation preferentially as a function of mantle thickness. This effect is ascribed to the limited effectiveness of vapor-pressure-induced water vapor diffusion up through small pores, a function of molecular mean-free-pathlength. Thermally-induced water vapor diffusion (Condition 2) shows a much smaller effect, asymptotically approaching the vapor-pressure "limit" at thick mantles for all particle sizes. Condition 1 (thermal and advective) components induce large sublimation rates, with larger particle sizes also enhancing sublimation even for thick mantles (smaller particle mantles loose their effectiveness at enhancing sublimation at thinner mantles).

A number of studies modeled the theoretical sublimation rates of ice, both exposed (e.g. Ingersoll, 1970; Wallace and Sagan, 1979; Haberle and Jakosky, 1990) and covered (e.g. Farmer, 1976; Clifford and Hillel, 1983; Zent et al., 1986), under a variety of martian conditions. The measured sublimation rates were compared to these works using the published formulae to calculate sublimation rates for conditions that matched those of the experiments.

The clean ice sublimation rate (J_c) was calculated using an expression employed by Ingersoll (1970) and subsequently used by many investigators, which as used in this study has the form:

$$J_c = 0.17\ (\Delta\rho)\ D_{om}[\ (\Delta\rho\ /\ \rho)\ g\ /\ \upsilon^{\,2}\ ]^{\,1/3}$$

where $\Delta\rho$ is the difference between total mixed-gas density at the surface and that of water vapor at the surface, $(\Delta\rho\ /\ \rho)$ is the ratio of the difference between mixed-gas density at the surface and that of water vapor at the surface to the mixed-gas density, D_{om} is the ordinary molecular diffusion coefficient for water vapor in CO_2, υ is the kinematic viscosity of CO_2, and g is the acceleration of gravity at the surface.

The rate of sublimation for ice under a dust cover (J_d) was calculated using an expression from Farmer (1976), also generally adopted by subsequent investigators. It has the form:

$$J_d = D_k\ V\ M_w\ /\ \Pi\ \kappa\ T\ L$$

where D_k is the Knudsen diffusion coefficient appropriate for the pore sizes within the dust layer, V is the saturation vapor pressure of ice for a given temperature, M_w is the molar mass of water, Π is Avagadro's number, κ is Boltzmann's constant, T is the temperature of the gas at the surface, and L is the thickness of the dust layer. The mean free path length of a mixture of H_2O and CO_2 at 3 mb at -20 °C was calculated to be 28 μm, which is an order of magnitude larger than the effective pore size (~1 μm) given in Clifford and Hillel (1983) for uncompressed, 10 μm diameter dust particles deposited from suspension. Gas diffusion through the dust layer is, as a consequence of the ratio of pore size to the mean free path length, entirely in the realm of Knudsen diffusion.

The calculations for both J_c and J_d assume that water vapor is subliming into a totally desiccated CO_2 atmosphere. To compare the theoretical predictions to the experimentally measured sublimation rate, the results from the environmental condition of the CO_2 gas circulating (via the operation of the circulation pump) over an isothermal sample were used.

The circulation pump cycled the entire volume of gas above the sample past the cold-finger and back to the chamber in approximately 70 seconds. This was equivalent to a surface "wind velocity" of roughly 1.5 cm/sec, a value only slightly higher than the rate at which H_2O vapor would be buoyantly lofted away from a surface in a still, dry CO_2 atmosphere.

Although experimental conditions should potentially be more conducive to ice sublimation than the theoretical conditions, just the opposite was actually the case: the experimentally-determined sublimation rate was one-sixth that calculated using the most common expression for clean ice sublimation rates (Ingersoll, 1970). The theoretical and actual values for the sublimation rate of ice under a dust cover appear to converge with increasing layer thicknesses. The sublimation rate of ice under 5 mm of dust had a measured value that was one-third the theoretical prediction.

The interpretation of these results are: 1) even thin layers of dust greatly lower the sublimation rate of an underlying ice substrate being heated from above, 2) thin layers of dust only mildly suppress the sublimation rate of an underlying ice substrate when samples are wholly isothermal, 3) even a low-flux, dry gas flow over a surface significantly increases the sublimation rate of any given sample, and 4) actual sublimation rates are within an order of magnitude but definitely lower than sublimation rates predicted from theoretical treatments.

Studies of Terrestrial and Martian Fluvial Processes

Studies of fluvial processes on Earth and Mars were a major research theme of the research supported by this contract and its predecessor grants at the Jet Propulsion Laboratory and Arizona State University (Malin 1976, 1978a, 1978b, 1978c, 1980, 1981, 1984, 1986, 1987, 1988, 1989; Sharp and Malin 1975; Mars Channel Working Group 1983; Malin and Eppler 1981; Malin et al. 1980; Pieri et al. 1980; Laity and Malin 1985; Laity et al 1980; Kelly and Malin 1988; Kelly et al 1988). The emphases of these varied investigations included age relationships (e.g., Malin 1976, 1978b), details of the processes of groudwater sapping (e.g., Malin et al 1980; Pieri et al 1980; Laity and Malin 1985), and catastrophic flood processes and sediment transport (e.g., Malin 1980, 1981, 1984, 1988, 1989; Malin and Eppler 1981). Below are summarized some of the conclusions drawn from the sapping and catastrophic flood studies.

Catastrophic Floods in Iceland

Catastrophic floods (jökulhlaups) of the Jökulsá á Fjöllum in north central Iceland have been examined by Thorarinsson (1950, 1959, 1960), Tómasson (1973), Sæmundsson (1973) and Einarsson (1976). These studies emphasized the hydrology of the JökuIsa á Fjöllum, the largest river in Iceland, and its potential for hydroelectric development. Among the aspects that suggested this potential was its relatively high and sustained yearly discharge and its deep canyon throughout most of its northern reach. However, it is this canyon, and the large, dry cataract Ásbyrgi, that brought to the forefront discussions of large jökulhlaups, for the canyon is tremendously underfit by the present river and its historic (fifteenth to eighteenth century) floods. Tómasson estimated discharges of ~4 x 10^5 m^3/sec, using several different methods, including assuming a canyon-filling flood and using the Manning equation and measurements of present day topography.

Photographic analysis and field work in the early- to mid-1980's revealed many of the large scale attributes of catastrophic floods shared by the Jökulsá á Fjöllum with the Channeled Scablands (formed by floods from Pleistocene Lake Missoula) and the Snake River canyon (formed by a flood from Pleistocene Lake Bonneville). Among these features are large, abandoned or severely underfit cataracts, "scabland" plucking of bedrock, broad lemniscate

forms, (principally erosional), occasional megaripples, and depositional tails behind large obstacles of many different sizes. Aside from the obvious transverse features associated with erosion (the scablands and cataracts), most of the landforms defining the course of the Jökulsá flood are primary depositional (e.g., depositional tails and boulder bars), or secondary erosion in deposits (e.g., waning stage channeling in previously deposited flood debris). Figure 2 (next page) shows a region of such landforms, the arrows pointing to the margin of an aa lava flow across which the flow behavior changes. The point at the extreme lower right corner of the photograph is seen in Figure 3 (next page) to have created a downstream bar of automobile-sized boulders.

Field work during the early- and mid-1980's emphasized physical measurement of landforms and debris. Examples of some of the results include observations of systematic debris caliber variations with longitudinal position and development of landforms characteristic of hydraulic conditions. Figure 4 (below, left) shows the longitudinal variation in mean size of the largest boulders. The increase at 110 km is associated with the area of scabland topography. Figure 4 (below, right) shows the size/frequency distribution of boulders in two boulder fields (the Selfoss/Dettifoss field was measured in an area of about 10^3 m^2, while the Krepputunga/Upptypingar was measured in an area of about 10^4 m^3). Note that all boulders were counted, so that the "drop off" at smaller sizes is not an observational problem--the population was deficient in smaller boulders. The shape of these curves indicates the sorting capability of the flood, and the sizes indicate the carrying capacity.

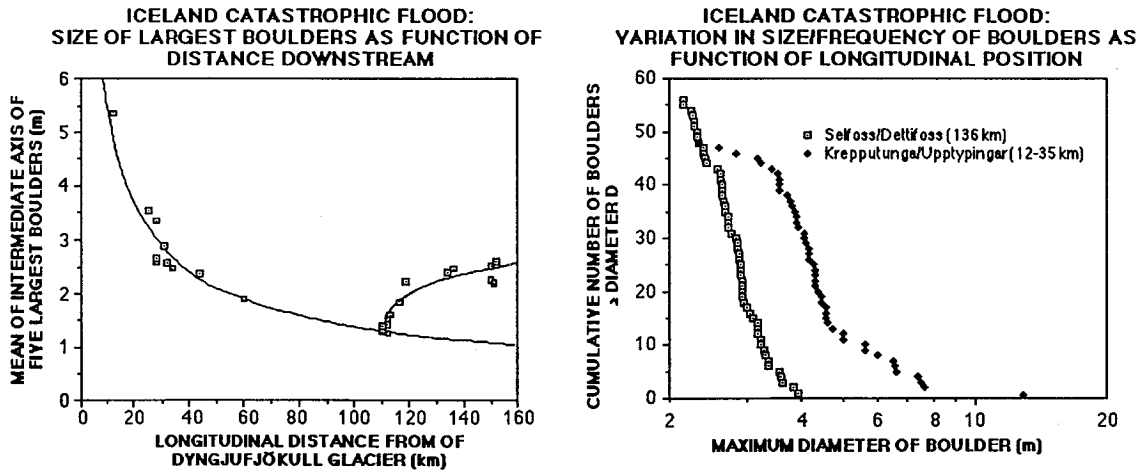

Figure 4: Longitudinal Variations in Boulder Populations

Several attributes of the flood permit characterization of flow parameters. For example, the planimetric form of Hrossaborg Crater (a maar volcano) was severely affected by the flood, and debris was deposited in specific sites around the crater. Figure 5 shows an aerial photograph of the crater. Figure 6, from Komar (1983), shows the variations in erosion of an erodable obstacle to flow of various hydraulic values, and Figure 7 shows sediment accumulated behind the inferred bow wave attachment point on Hrossaborg Crater. These relationships suggest sub-critical flow (Froude number ~0.4), consistent with a velocity of ~4-5 m/sec, a flow depth of ~20 m, and a discharge of roughly 4 X 10^5 m^3/sec.

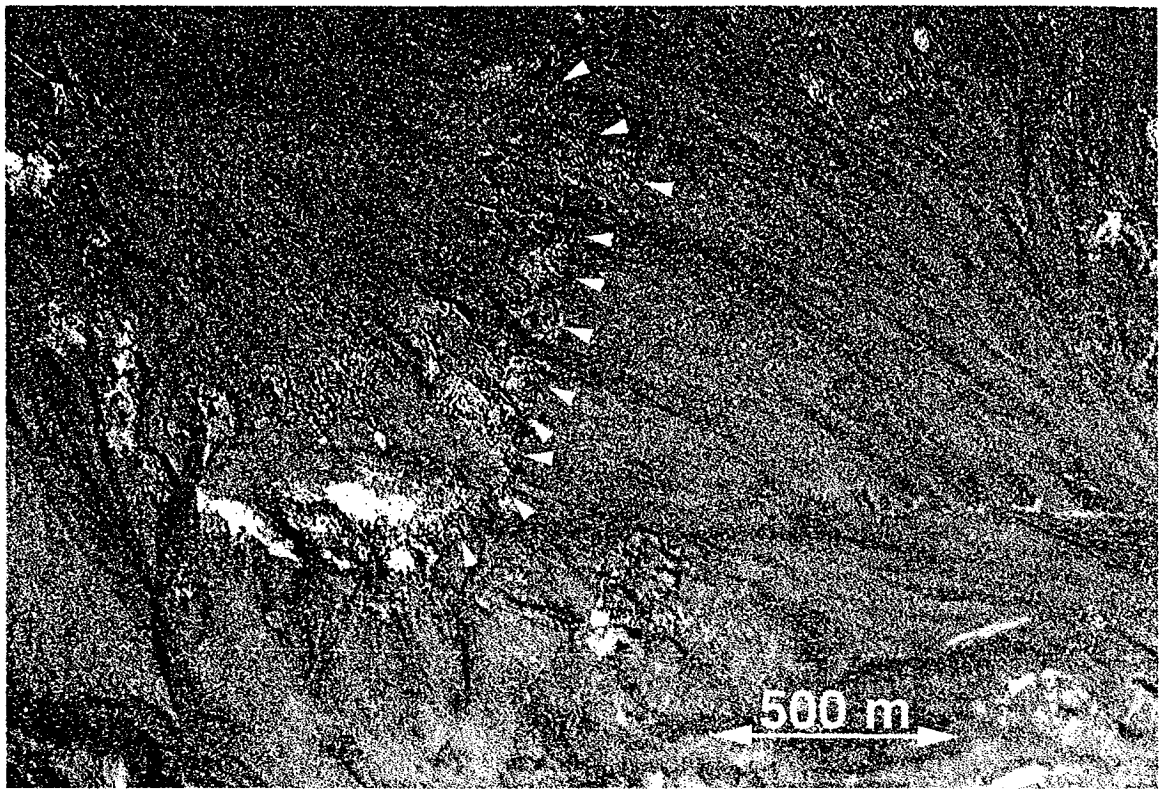

Figure 2: Krepputunga reach of Jökulsá á Fjöllum Flood

Figure 3: Boulder Bar formed as flood descended across Aa lava flow. Located in lower right corner of Figure 2.

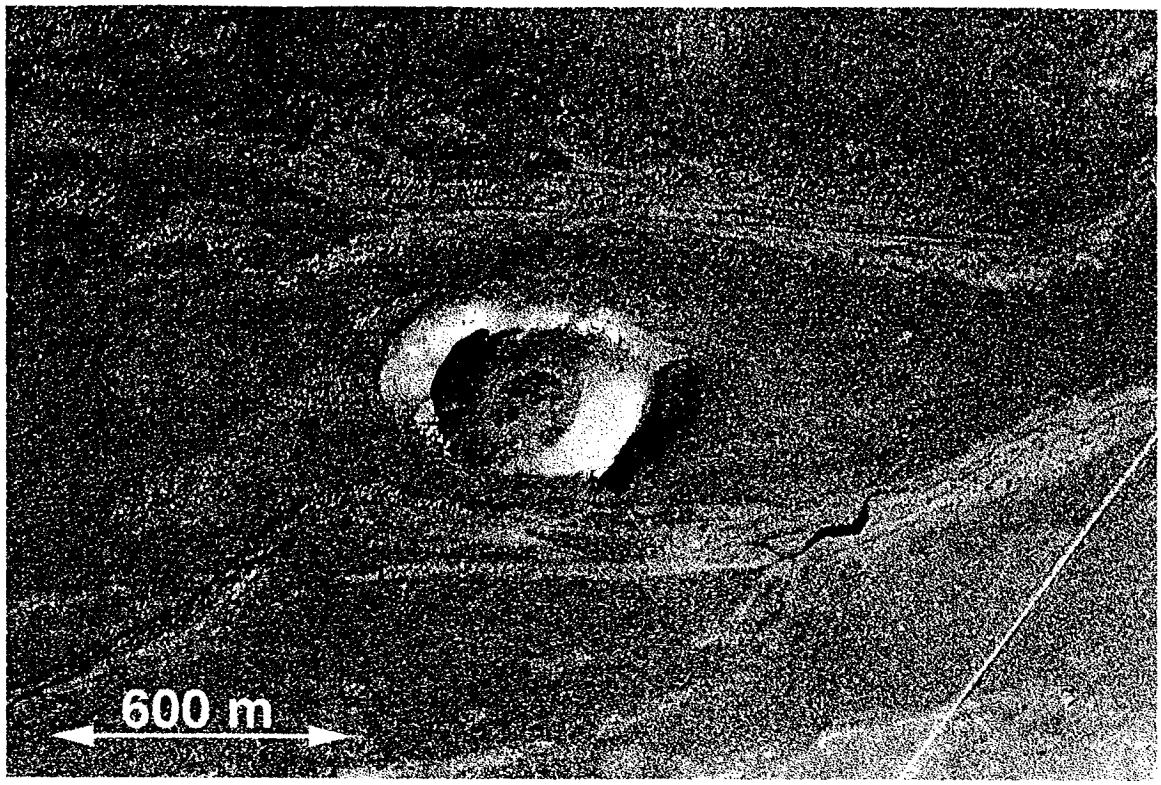

Figure 5: Hrossaborg Crater, approximately 600 m in diameter, eroded by flood.

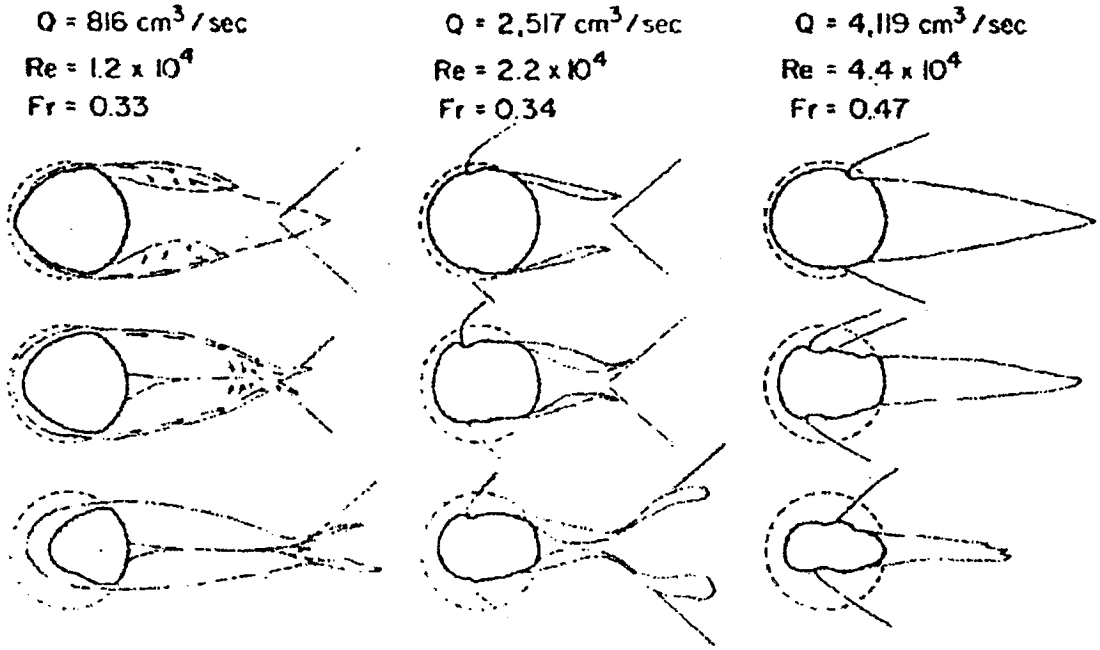

Figure 6: Results of several flume runs with discharges as noted and flow thicknesses just less than obstacle height (approximately 3 cm). Note erosion of portions of obstacle transverse to the flow, and the accumulation of depositional lobes. From Komar, 1983

Figure 7: Lateral bar east of breach in Hrossaborg Crater wall. Note person for scale (arrow)

Additional estimates of discharge were made in several areas based on plunge pool geometry, splash marks, and Manning calculations. Peak discharge in areas where a single channel was occupied were remarkably consistent, with values between about 5-6 X 10^5 m^3/sec in proximal locations and values closer to 3 X 10^5 m^3/sec at Ásbyrgi, approximately 130 km distal.

Megaripples are not ubiquitous. Although they are found primarily along the margin of the most deeply eroded scablands, at least one set is clearly truncated by the development of the scablands, suggesting multiple phases to the development of the canyon. The best developed set, seen in Figure 8 and 9, is variable in wavelength and amplitude (both becoming larger downstream - to the right in Figure 8). This set had an average wavelength of 20 m , an amplitude of 1.5 m , and were composed of material principally between 2 and 10 cm diameter (largest ~ 1.5 m)(Figure 9).

A number of conclusions relevant to martian outflow channels were drawn from observations of the Jökulsá á Fjöllum flood. Sedimentary processes dominate erosional processes away from canyon walls. Boulder fields occur in specific locations or in large areas of common hydraulic properties; large boulders in some areas may be extremely abundant. However, high areal density of boulders is relatively rare. Much of the relief in affected areas is low; slopes away from cataracts and scablands are typically much less than 1°.

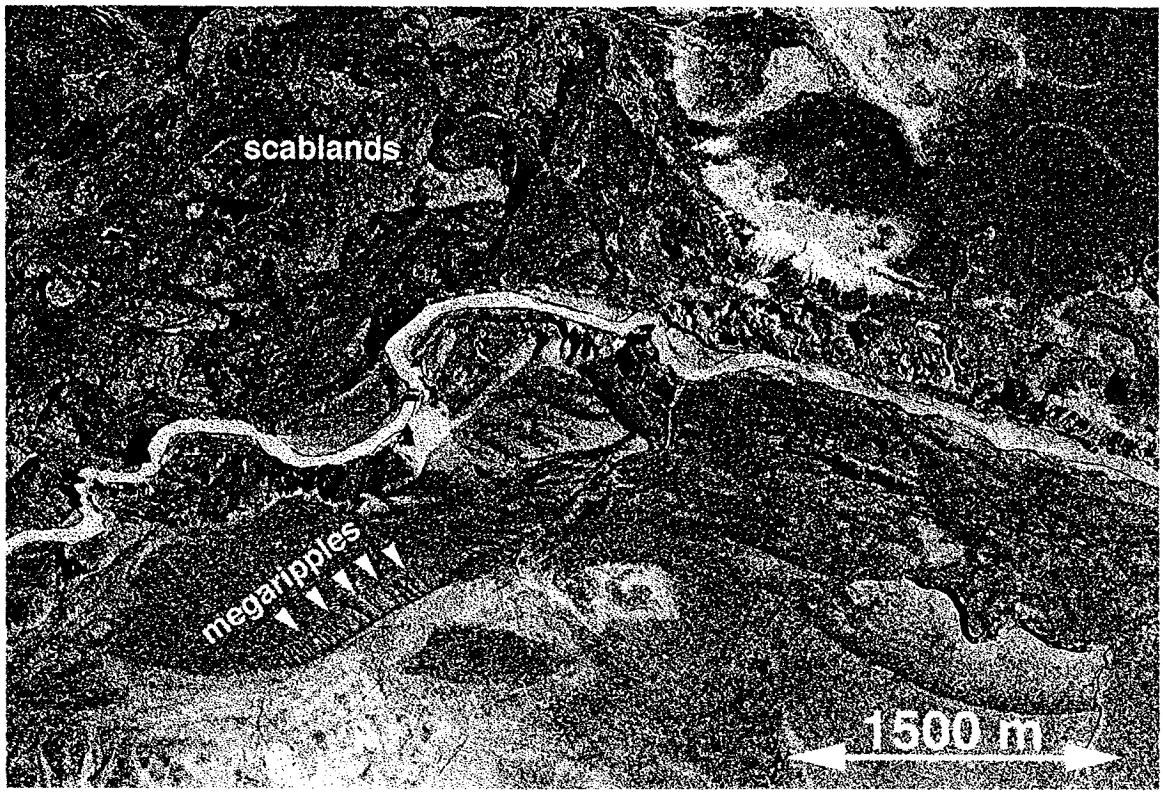

Figure 8: Vesturdalur scablands, also showing well developed "megaripples."


Figure 9: Ground view of Vesturdalur "megaripples."